F.T.M.N., and J.W.), Deutsche Forschungsgemeinschaft (H.F. and B.E.), the Engineering and Physical Sciences Research Council (H.W. and R.R.K.) and the NSF (F.W.). Part of the experimental equipment was supplied by La Vision GmbH.

Supporting Online Material
www.sciencemag.org/cgi/content/full/305/5690/1594/DC1
Materials and Methods
Figs. S1 to S8
Tables S1 and S2
References

17 May 2004; accepted 30 July 2004

Mesophase Structure-Mechanical and Ionic Transport Correlations in Extended Amphiphilic Dendrons

B.-K. Cho,[1]* A. Jain,[1]* S. M. Gruner,[2] U. Wiesner[1]†

We have studied the self-assembly of amphiphilic dendrons extended with linear polyethylene oxide (PEO) chains and their ion complexes. Keeping the dendron core and linear PEO chain compatible allows for the combination of dendritic core-shell and conventional block copolymer characteristics for complex mesophase behavior. An unexpected sequence of crystalline lamellar, cubic micellar ($Pm\bar{3}n$), hexagonal columnar, continuous cubic ($Ia\bar{3}d$), and lamellar mesophases is observed. Multiple phase behavior within single compounds allows for the study of charge transport and mechanical property correlations as a function of structure. The results suggest an advanced molecular design concept for the next generation of nanostructured materials in applications involving charge transport.

The generation of supramolecular structures by self-assembly of molecular building blocks has become a powerful tool in designing enhanced material properties (*1*, *2*). Molecular engineering of the interface in microphase-separated domains is believed to be a key to the precise manipulation of supramolecular structures. To this end, a variety of molecular building blocks with rod (*3*), disk (*4*), and linear (*5*) type architecture have already been combined. Recently, dendrimers and their segments, dendrons, have fostered scientific interest as another class of building blocks. They are attractive because their particular shape introduces curved interfaces and because large numbers of functional groups can be readily introduced into a single molecule (*6*–*8*). Their unique structural features might lead to phase behavior that is quite different from that of conventional linear building blocks (*9*). Indeed, the dendrimer/dendron-periphery interface has been systematically controlled by either tethering different generations or periphery groups (*10*–*12*), and micellar structures with complicated lattices have been found in benzyl ether–based dendrons as a function of temperature (*13*, *14*). Despite theoretical predictions of a rich phase behavior (*15*), observed phases to date reveal only lamellar, columnar, or micellar packing. In particular, the existence of three-dimensional (3D) cubic network structures important for potential applications has not been demonstrated.

Here we report on third-generation amphiphilic dendrons extended by linear polyethylene oxide (PEO) chains synthesized as described in (*16*). Although several molecules with varying PEO molecular weights were studied, we will focus on two compounds, **1** and **2** (Fig. 1), which exhibit multiple phases that combine the behavior of linear block copolymers with that of dendritic systems. The mesophases were accessible through temperature changes and include crystalline lamellar (k_1, k_2), micellar (mc), hexagonal columnar (hex), continuous cubic (cc), lamellar (lam), and disordered (dis). Molecular masses of compounds **1** and **2** were determined to be 4600 and 7500 g/mol by matrix-assisted laser desorption ionization time-of-flight (MALDI-TOF) mass spectrometry. Based on these molecular masses and the density of each block, the hydrophilic volume fractions (f) were calculated to be 0.41 and 0.62 for **1** and **2**, respectively. Polydispersities (M_w/M_n) from MALDI-TOF mass spectrometry and gel permeation chromatography (GPC) were found to be less than 1.05. In contrast to most previous combinations of coil-dendron systems, the interface of these linearly extended dendrons is modeled in the middle of the dendritic structure rather than at the focal point (*17*–*20*). The hydrophilic part is composed of linear PEO plus a PEO-like dendritic core, whereas the hydrophobic fraction consists of eight docosyl peripheries (*21*, *22*). In this way, structural features of phase-separated dendritic core-shell architectures are combined with the ability to fine tune volume fractions through simple linear chain extension. Furthermore, linear and branched chain topologies are combined within one domain of the microphase-separated material.

Thermal behavior of compounds **1** and **2** was studied by differential scanning calorimetry (DSC) and transitions corroborated by dynamic mechanical spectroscopy (DMS) and temperature-dependent small-angle x-ray scattering (SAXS). The results are summarized in Table 1. DSC was run at a rate of 10°C/min, and transition temperatures were determined at peak maxima. Isochronal temperature step measurements at a frequency of 0.5 rad/s and shear amplitude in the linear regime (<2%) were performed on an advanced rheometrics expansion system (ARES) to identify the melting temperatures of the docosyl peripheries, order-order transitions (OOTs), and order-disorder transitions (ODTs). In DSC data, **1** and **2** show two

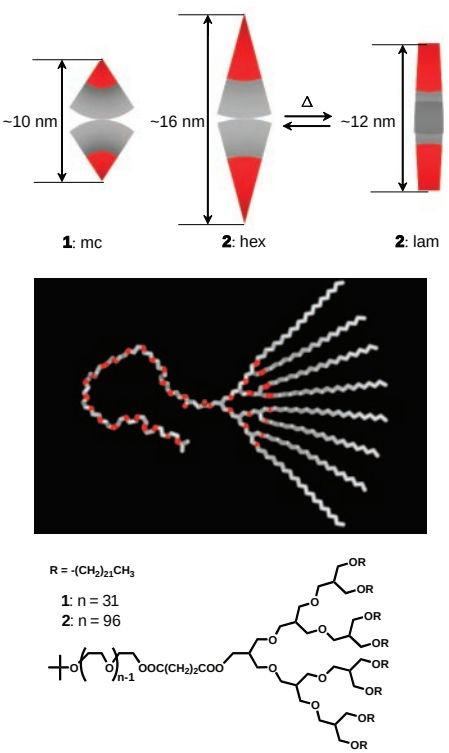

Fig. 1. Molecular architecture of extended amphiphilic dendrons **1** and **2**. Oxygen-containing segments are shown in red. (**Top**) Schematics of the type of molecular packing in different mesophases along with the respective dimensions consistent with SAXS data analyses and molecular models (red, hydrophilic parts; gray, hydrophobic parts). The schematics are meant to illustrate aspects of the local packing behavior only.

Department of Materials Science and Engineering and [2]Department of Physics, Cornell University, Ithaca NY 14853.
*These authors contributed equally to this work.
†To whom correspondence should be addressed. E-mail: ubw1@cornell.edu

distinct transitions corresponding to melting of the linear PEO chains and docosyl peripheries. Upon further heating, both **1** and **2** form ordered mesophases and subsequently disordered liquids.

All ordered microstructures were characterized using temperature-variable SAXS experiments. A summary of measured distances and corresponding indexation for each mesophase is given in Table 2. The extended amphiphilic dendrons are all consistent with lamellar structures in the crystalline states (Fig. 2B). After PEO (12°C) and periphery (63°C) melting and before isotropization, the SAXS pattern of **1** shows a large number of reflections (Fig. 2A). They can be indexed consistently as a cubic structure with $Pm\bar{3}n$ symmetry. After melting (45°C PEO, 63°C periphery), **2** shows three distinct mesophases as a function of temperature before isotropization. For the first mesophase, the SAXS pattern shows five reflections, consistent with a hexagonal mesophase (Fig. 2C). As the temperature increases, two intense and several weak reflections appear (Fig. 2D), consistent with a cubic structure of $Ia\bar{3}d$ symmetry. Upon further heating, **2** displays two reflections with a q-spacing ratio of 1:2. Although only two peaks are seen, the equal spacing between the peaks and the occurrence at relatively large angles are suggestive of a lamellar mesophase (Fig. 2E).

Despite an intermediate hydrophilic volume fraction $f = 0.41$ of **1**, the cubic mesophase with $Pm\bar{3}n$ symmetry is expected to be a micellar structure (Fig. 3A). This is consistent with the observation that **2,** with higher $f = 0.62$, shows a columnar mesophase after melting (Fig. 3C). In the micellar mesophase, the hydrophilic parts occupy the core encapsulated by the hydrophobic peripheries, as expected from the inherent interfacial curvature. Cubic structures with $Pm\bar{3}n$ symmetry have been found in only a few bulk systems with other molecular structures such as taper-shaped small amphiphiles and cone-shaped dendrons (*23*–*25*), and have recently been predicted for branched block copolymer type systems (*15*).

Most notable, however, is the cubic mesophase with $Ia\bar{3}d$ symmetry at intermediate temperatures of **2**. In Fig. 3D, this symmetry is represented by a gyroidlike continuous structure, consistent with conductivity measurements and theoretical predictions for linear-branched block copolymers (*15*). In contrast, dendrimers/dendrons have mostly been shown to self-organize into columnar or micellar structures due to their taper/cone-shaped molecular architecture (*24*–*27*). Furthermore, the mesophase sequence in which the $Ia\bar{3}d$ phase is observed upon heating—i.e., hexagonal, $Ia\bar{3}d$, lamellar, disordered—is quite unusual for block copolymers. It is not readily understood in the context of simple diblock copolymer phase diagrams (*15*, *28*). The sequence is likely due to a larger expansion parallel to the interface as a function of temperature of the linear PEO/branched (dendritic) section of the molecules versus the hydrophobic docosyl section. The effect thus may be explained by similar arguments governing packing of surfactant molecules (Fig. 1) (*29*).

The linear viscoelastic properties of soft materials are sensitive to morphology. Measurements of the temperature dependence of the elastic shear modulus (G') with a dynamic mechanical spectrometer are in good agreement with the results of DSC and SAXS studies. In Fig. 4A, after a large drop from the crystalline lamellar phase, the cubic mesophase with $Pm\bar{3}n$ symmetry of **1** shows high G' values ($\sim 10^6$ Pa), which can be attributed to the 3D cubic symmetry (*30*). Upon heating into the disordered state, the modulus drops precipitously. In the case of **2**, G' values nicely follow the transitions as observed by DSC and/or SAXS and, after melting, are highest for the intermediate $Ia\bar{3}d$ cubic structure, which shows elastic behavior similar to that of the $Pm\bar{3}n$ phase of **1** (Fig. 4B). Despite the lower temperatures, the hexagonal phase exhibits almost an order of magnitude lower G' values. At higher temperatures, values drop more than two orders of magnitude into the lamellar phase, before they finally plummet upon heating into the disordered phase.

A powerful tool for elucidating structural features like dimensionality and connectivity is measuring the transport behavior within one domain of the phase-separated material (*31*, *32*). To this end, we prepared ion-doped extended amphiphilic dendrons **1-Li$^+$** and **2-Li$^+$**, adding lithium triflate salt that is selectively soluble in the hydrophilic parts. To ensure minimal deviations in volume fraction from undoped **1** and **2**, we chose Li^+ concentrations per ethylene oxide to be 0.02. The transition temperatures of ion-doped materials were first characterized by DSC, DMS, and SAXS (Table 1). Whereas the melting transitions, as observed by DSC, were essentially unchanged, ion-doping stabilized the mesophases, resulting in a high-temperature shift of the transition temperatures (Fig. 4, A and B). The stabilization of both the mc phase of **1** and the hex phase of **2** by about 50°C can be attributed to the increased interaction parameter, χ, upon doping with lithium salts. It may also be due to the rigidifying of the PEO chains upon Li^+ addition. Surprisingly, for **2-Li$^+$** at temperatures above 170°C, SAXS diffractograms are obtained that are consistent with a cubic mesophase with $Ia\bar{3}d$ symmetry (Fig. 2F). This is in marked contrast to the case of linear block copolymers (*33*), in which even small amounts of polar ions have been shown to force the system into a stronger segregation regime, causing a switch from an $Ia\bar{3}d$ bicontinuous cubic phase to a hexagonal columnar mesophase. The lamellar mesophase and isotropic liquid phase of **2** are not reached because ion-doped extended dendrons begin to degrade near 195°C, as observed by thermal gravimetric analysis (*34*).

Ionic conductivity was measured with an impedance analyzer in the frequency range of 10^1 to 10^6 Hz. Direct conductivity was obtained by extrapolation to zero frequency (*35*). In Fig. 4C, the changes in conductivity as a function of temperature for ion-doped

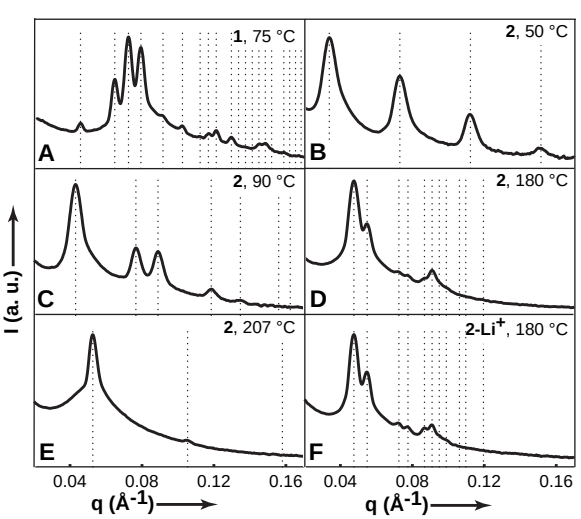

Fig. 2. SAXS spectra for **1** (**A**), **2** (**B** to **E**), and **2-Li$^+$** (**F**) at different temperatures plotted against the scattering wave vector, q ($= 4\pi\sin\theta/\lambda$). The vertical dotted lines correspond to the expected peaks for $Pm\bar{3}n$ cubic (A), lamellar (B and E), hexagonal columnar (C), and $Ia\bar{3}d$ cubic (D and F) lattices.

Table 1. Phase behavior of **1**, **2**, **1-Li$^+$**, and **2-Li$^+$**. k, crystalline; mc, micellar; hex, hexagonal columnar; lam, lamellar; cc, continuous cubic; dis, disordered; dec, decomposition.

Compound	Phase transitions (°C)
1	k_1 12 k_2 63 mc 93 dis
2	k_1 45 k_2 63 hex 114 cc 190 lam 226 dis
1-Li$^+$	k_1 16 k_2 63 mc 139 dis
2-Li$^+$	k_1 44 k_2 63 hex 170 cc 195 dec

compounds **1-Li**$^+$ and **2-Li**$^+$ are in excellent agreement with the temperature-dependent behavior as observed by DSC (Table 1) and DMS (Fig. 4, A and B). For **1-Li**$^+$, the most interesting feature in the conductivity curve occurs at the docosyl periphery melt transition where the conductivity drops from 4.6 $\times 10^{-6}$ to 1.2 $\times 10^{-9}$ S/cm. This large reduction in the conductivity is consistent with the interpretation of a 2D layer structure melting into a micellar structure in which hydrophilic micelles are embedded in a hydrophobic matrix (Fig. 3, A and B). Thus, lithium ions are preferentially confined in micelles, preventing fast long-range transport. The huge conductivity drop by more than three orders of magnitude at the transition can potentially be used as a supramolecular on-off switch. Indeed, the mechanical properties (G′ $\sim 10^6$ Pa) of this micellar mesophase are sufficient to encourage such an application (Fig. 4A). Interestingly, no discontinuity is observed for **1-Li**$^+$ upon disordering at 139°C. This is consistent with recent studies of the order-disorder transition (ODT) in sphere-forming diblock copolymer melts, demonstrating that at the transition, the long-range order (or lattice) of micelles disappears whereas micelles persist up to much higher temperatures (*36*, *37*).

The most complex transport behavior is found for **2-Li**$^+$, with four different conductivity regimes strongly correlated to the mesophase behavior of this compound. At the first melting transition (PEO), conductivity rises by one to two orders of magnitude, whereas at the second (periphery melting), it drops by about an order of magnitude, going from a crystalline lamellar into the hexagonal mesophase. At the onset of the $Ia\bar{3}d$ cubic mesophase, it rises again by an order of magnitude and finally reaches values of about 1.5 $\times$ 10^{-4} S/cm at the highest temperatures measured. The observation of a distinct step in conductivity upon PEO melting for **2-Li**$^+$, which was not observed for **1-Li**$^+$, is consistent with a substantially increased degree of crystallinity for this compound due to the longer PEO chains. All other transition behavior can be rationalized by assuming that the hydrophilic parts responsible for ion transport form cylinder cores in both the hexagonal and cubic mesophases, because the conductivity in the present nonaligned microstructures is then expected to be roughly proportional to the dimensionality of the structure (*38*). Following this argument, periphery melting leads to a transition from a 2D lamellar to a 1D hexagonal columnar phase, resulting in a sharp decrease in the ion conductivity. The transition into the cubic phase increases the dimensionality to three, resulting in the highest conductivity values of about 1.5 $\times$ 10^{-4} S/cm. This analysis also reveals that the $Ia\bar{3}d$ cubic structure is continuous. We note that the present conductivity values of the cubic structure without macroscopic orientation efforts are comparable to those of aligned lamellar structures at similar temperatures and lithium concentrations (*39*, *40*). Furthermore, this mesophase shows outstanding mechanical properties (G′ $\sim 10^6$ Pa for **2-Li**$^+$) as expected for a continuous structure (Fig. 4B), making it particularly attractive for applications involving charge transport.

In conclusion, we have demonstrated that the present extended amphiphilic dendrons self-assemble into an unexpected sequence of crystalline lamellar, $Pm\bar{3}n$ micellar cubic, hexagonal columnar, $Ia\bar{3}d$ continuous cubic, and lamellar mesophases as a function of volume fraction and temperature. We revealed local core-shell topologies by monitoring the ion conductivity of ion-doped samples, which is strongly correlated to mesophase behavior and mechanical properties. We were thus able to study charge transport within a nanostructured material in which the conducting medium is confined to either micelles (zero-dimensional), cylinders (1D), or lamellae (2D), or is a continuous (3D) network throughout the entire macroscopic sample (Fig. 3). These results may

Table 2. The measured distances ($d_{meas} = 2\pi/q$; see Fig. 2 legend) and corresponding (*hkl*) indexation data of the observed SAXS reflections for each mesophase. d_{calcd} is the calculated distance based on the lattice parameter of each structure. Depending on the strength of the peak, the accuracy of measurement is generally better than 0.5 Å.

hkl	d_{meas} (Å)	d_{calcd} (Å)
$Pm\bar{3}n$ cubic structure with lattice parameter of 194.0 Å in Fig. 2A		
110	137.2	137.2
200	97.0	97.0
210	86.8	86.8
211	79.2	79.2
220	69.0	68.7
310	61.5	61.4
320	53.7	53.8
321	51.9	51.9
400	48.5	48.5
420	43.4	43.4
421	42.3	42.3
2D hexagonal structure with lattice parameter of 162.2 Å in Fig. 2C		
100	140.5	140.5
110	81.1	81.1
200	70.1	70.3
210	53.1	53.1
$Ia\bar{3}d$ cubic structure with lattice parameter of 324.4 Å in Fig. 2D		
211	132.3	132.3
220	114.9	114.7
321	87.4	86.7
400	81.6	81.1
420	72.4	72.5
332	69.2	69.1
Lamellar structure with lattice parameter of 119.2 Å in Fig. 2E		
100	119.2	119.2
200	59.9	59.6

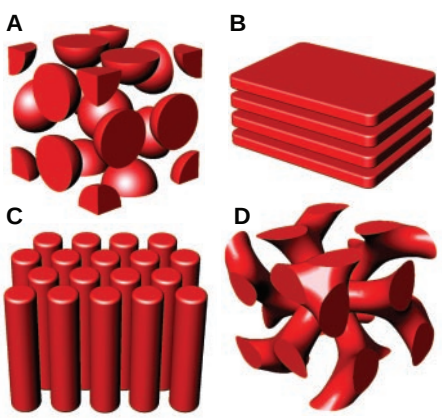

Fig. 3. Schematic illustration of supramolecular architectures of self-assembled extended amphiphilic dendrons consistent with the various lattice symmetries: $Pm\bar{3}n$ cubic (micelles) (**A**), lamellar (2D layers) (**B**), hexagonal columnar (1D cylinders) (**C**), and $Ia\bar{3}d$ continuous cubic (3D network) (**D**) structures. The red-colored parts represent the hydrophilic domains consisting of PEO chains and dendritic cores in which, for lithium-doped compounds, the ion transport takes place.

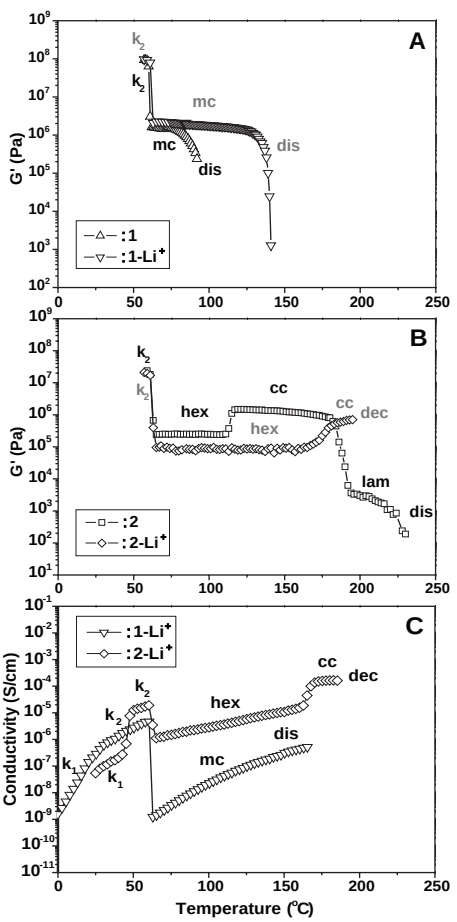

Fig. 4. Elastic modulus G′ (**A** and **B**) and ionic conductivity (**C**) as a function of temperature for extended amphiphilic dendrons **1** and **2** and their ion-doped **1-Li**$^+$ and **2-Li**$^+$. Mesophase nomenclature is given in Table 1.

have significant implications in areas where charge transport in nanostructured materials and devices is becoming increasingly important, such as ion conductors, photovoltaics or electroluminescence, for which the present extended amphiphilic dendrons may provide an advanced molecular design concept.

References and Notes

1. J. M. Lehn, *Supramolecular Chemistry* (VCH, Weinheim, Germany, 1995).
2. V. Percec *et al*., *Nature* **417**, 384 (2002).
3. S. I. Stupp *et al*., *Science* **276**, 384 (1997).
4. D. Demus, J. Goodby, G. W. Gray, H. W. Spiess, V. Vill, *Handbook of Liquid Crystals* (Wiley-VCH Verlag, Weinheim, Germany, 1998).
5. M. A. Hillmyer *et al*., *Science* **271**, 976 (1996).
6. C. J. Hawker, J. M. J. Fréchet, *J. Am. Chem. Soc.* **112**, 7638 (1990).
7. D. A. Tomalia *et al*., *Polym. J.* **17**, 117 (1985).
8. E. W. Buhleier, W. Wehner, F. Vögtle, *Synthesis* 155 (1978).
9. A. W. Bosman, H. M. Janssen, E. W. Meijer, *Chem. Rev.* **99**, 1665 (1999).
10. V. S. K. Balagurusamy, G. Ungar, V. Percec, G. Johansson, *J. Am. Chem. Soc.* **119**, 1539 (1997).
11. K. Lorenz, H. Frey, B. Stühn, R. Müllhaupt, *Macromolecules* **30**, 6860 (1997).
12. J. H. Cameron, A. Facher, G. Lattermann, S. Diele, *Adv. Mater.* **9**, 398 (1997).
13. G. Ungar, Y. Liu, X. Zeng, V. Percec, W. D. Cho, *Science* **299**, 1208 (2003).
14. X. Zeng *et al*., *Nature* **428**, 157 (2004).
15. G. M. Grason, B. A. DiDonna, R. D. Kamien, *Phys. Rev. Lett.* **91**, 58304 (2003).
16. B.-K. Cho *et al*., *J. Am. Chem. Soc.* **126**, 4070 (2004).
17. I. Gitsov, K. L. Wooley, C. J. Hawker, P. T. Ivanova, J. M. J. Fréchet, *Macromolecules* **26**, 5621 (1993).
18. M. A. Johnson, J. Iyer, P. T. Hammond, *Macromolecules* **37**, 2490 (2004).
19. C. Román, H. R. Fischer, E. W. Meijer, *Macromolecules* **32**, 5525 (1999).
20. M. E. Mackey *et al*., *Macromolecules* **35**, 8391 (2002).
21. M. Jayaraman, J. M. J. Fréchet, *J. Am. Chem. Soc.* **120**, 12996 (1998).
22. B.-K. Cho *et al*., *Macromolecules* **37**, 4227 (2004).
23. K. Borisch, S. Diele, P. Göring, C. Tschierske, *Chem. Commun*. 237 (1996).
24. S. D. Hudson *et al*., *Science* **278**, 449 (1997).
25. V. Percec *et al*., *Nature* **391**, 161 (1998).
26. S. M. Grayson, J. M. J. Fréchet, *Chem. Rev.* **101**, 3819 (2001).
27. D. Tsiourvas, K. Stathopoulou, Z. Sideratou, C. M. Paleos, *Macromolecules* **35**, 1746 (2002).
28. I. W. Hamley, *The Physics of Block Copolymers* (Oxford Univ. Press, New York, 1998).
29. J. N. Israelachvili, D. J. Mitchell, B. W. Ninham, *J. Chem. Soc. Faraday Trans.* **1**, 72, 1525 (1976).
30. J. Zhao *et al*., *Macromolecules* **29**, 1204 (1996).
31. P. P. Soo *et al*., *J. Electrochem. Soc.* **146**, 32 (1999).
32. P. V. Wright, Y. Zheng, D. Bhatt, T. Richardson, G. Ungar, *Polym. Int.* **47**, 34 (1998).
33. T. H. Epps, T. S. Bailey, R. Waletzko, F. Bates, *Macromolecules* **36**, 2873 (2003).
34. B.-K. Cho, A. Jain, S. M. Gruner, U. Wiesner, data not shown.
35. H. Kosonen *et al*., *Macromolecules* **35**, 10149 (2002).
36. E. E. Dormidontova, T. P. Lodge, *Macromolecules* **34**, 9143 (2001).
37. X. Wang, E. E. Dormidontova, T. P. Lodge, *Macromolecules* **35**, 9687 (2002).
38. J. Ruokolainen *et al*., *Science* **280**, 557 (1998).
39. T. Ohtake *et al*., *Chem. Mater.* **12**, 782 (2000).
40. K. Kishimoto *et al*., *J. Am. Chem. Soc.* **125**, 3196 (2003).

41. This work was supported by the Postdoctoral Fellowship Program of Korea Science and Engineering Foundation (KOSEF), the NSF (DMR-0312913), and the Cornell Center for Materials Research (CCMR), a Materials Research Science and Engineering Center (MRSEC) of the NSF (DMR-0079992). Financial support of Philip Morris, USA, is gratefully acknowledged. The SAXS x-ray facility is supported by Department of Energy Biological and Environmental Research (BER) grant DE-FG02-97ER62443. This work made use of the CCMR Hudson mesoscale facility, supported through the NSF MRSEC Program (DMR-0079992). We thank H. J. Räder and S. Türk (Max-Planck Institute for Polymer Research) for the MALDI-TOF measurements on the extended dendrimers and S. Mahajan (Cornell University) for help with PEO synthesis.

28 May 2004; accepted 12 August 2004

DNA-Templated Organic Synthesis and Selection of a Library of Macrocycles

Zev J. Gartner, Brian N. Tse, Rozalina Grubina, Jeffrey B. Doyon, Thomas M. Snyder, David R. Liu*

The translation of nucleic acid libraries into corresponding synthetic compounds would enable selection and amplification principles to be applied to man-made molecules. We used multistep DNA-templated organic synthesis to translate libraries of DNA sequences, each containing three "codons," into libraries of sequence-programmed synthetic small-molecule macrocycles. The resulting DNA-macrocycle conjugates were subjected to in vitro selections for protein affinity. The identity of a single macrocycle possessing known target protein affinity was inferred through the sequence of the amplified DNA template surviving the selection. This work represents the translation, selection, and amplification of libraries of nucleic acids encoding synthetic small molecules rather than biological macromolecules.

Nature generates functional biological molecules by subjecting libraries of nucleic acids to iterated cycles of translation, selection, amplification, and diversification (*1*–*4*). Compared with analogous synthesis and screening methods currently used to discover synthetic molecules with desired properties, these evolution-based approaches are attractive because of the much larger numbers of molecules that can be simultaneously evaluated, the minute quantities of material needed, and the relatively modest infrastructure requirements for library synthesis and processing (*1*–*4*).

Despite these attractions, evolution-based approaches can only be applied to molecules that can be translated from amplifiable information carriers. We previously described the generality of DNA-templated organic synthesis (DTS) and explored its potential for translating DNA sequences into corresponding synthetic products by using DNA hybridization to modulate the effective molarity of DNA-linked reactants (*5*). DTS can generate products unrelated in structure to the DNA backbone in a sequence-specific manner (*5*, *6*), does not require functional group adjacency to proceed efficiently (*5*, *7*), can mediate sequence-programmed multistep small-molecule synthesis (*8*), and can enable reaction pathways that are difficult or impossible to realize with the use of conventional synthetic strategies (*9*).

These features of DTS raise the possibility of translating single-solution libraries of DNA sequences into corresponding libraries of synthetic small molecules conjugated to their respective templates. Because each member of a DNA-templated synthetic library is linked to an encoding nucleic acid, these libraries are suitable for in vitro selection (*10*), polymerase chain reaction (PCR) amplification, and DNA sequence characterization to reveal the identity of synthetic library members possessing functional properties (Fig. 1). Below, we describe the integration of these concepts into the DNA-templated synthesis of a library of macrocycles (Fig. 2A), the selection of this pilot library for affinity to a target protein, and the identification of a functional library member through the amplification and characterization of DNA sequences surviving the selection.

Although macrocycles can be challenging targets for conventional synthesis (*11*), the compatibility of DTS with nM reactant concentrations, aqueous solvents (*12*), and purification methods not available to conventional synthesis (*8*) suggested that macrocycle synthesis might proceed efficiently in this format. We subjected a 48-base DNA-linked lysine derivative (**1a**, the "template," analogous to an mRNA during protein biosynthesis) to three successive DNA-templated amine acylation reactions (*6*) with building blocks conjugated to DNA 10-mer or 12-mer oligonucleotides (**2a**, **3a**, or **4a**, the "re-

Department of Chemistry and Chemical Biology, Harvard University, 12 Oxford Street, Cambridge, MA 02138, USA.

*To whom correspondence should be addressed. E-mail: drliu@fas.harvard.edu

edited by Stella Hurtley and Phil Szuromi

Composition of Jupiter's Atmosphere

When the Cassini spacecraft flew by Jupiter on its way to Saturn, the Composite Infrared Spectrometer (CIRS) took measurements of the jovian upper atmosphere. **Kunde *et al.*** (p. 1582, published online 19 August 2004) found enhancements of some hydrocarbons in the aurorae associated with temperature and magnetic field effects. Carbon dioxide and hydrogen cyanide added to the stratosphere by the impact of comet Shoemaker-Levy 9 have not been transported or diffused very much, possibly because polar vortices are inhibiting the diffusion of these species to higher latitudes.

Macrocyclic Libraries via DNA

DNA recognition has been exploited in several ways to synthesize libraries of macrocycles. **Gartner *et al.*** (p. 1601, published online 19 August 2004) linked single-stranded DNA to the peptide-like building blocks of macrocycles. DNA recognition of complementary strands brought the ring components into proximity so that ring-closure reactions could be performed. Specific macrocycles can then be selected for their protein affinity or enzymatic inhibition, and then identified by amplifying their DNA tags. A library of 65 such compounds was constructed.

Dendrimeric Diblock Copolymers

Diblock copolymers can phase-separate into a rich array of morphologies, and dendrimer polymers allow many different functionalities to be placed onto highly branched compact molecules. **Cho *et al.*** (p. 1598) combined these two architectures into a single molecule and examined the phase behavior of a dendron grafted onto a long linear chain segment. The molecules show the same spherical, cylindrical, and lamellar structures seen in normal diblock copolymers, but also an unusual continuous cubic structure. The mechanical and charge transport properties of the polymers could be correlated with the observed phases.

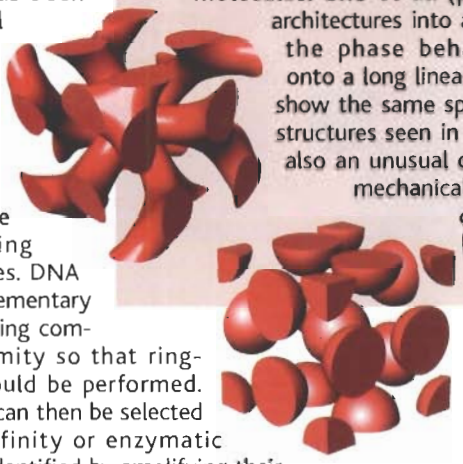

Suddenly Turbulent

Despite having been studied for more than 100 years, the transition from laminar to turbulent flow in pipes is not understood. For other flow geometries, the source of the initial instabilities can be identified, but theory predicts that pipe flow should remain laminar for all flow rates. Recent numerical calculations suggested that traveling waves may be the reason the flow becomes turbulent. **Hof *et al.***'s (p. 1594; see the Perspective by **Busse**) hypothesis is now confirmed through experimental observations.

Slippery But Still Wet

The hydrophobic effect (the poor solvation of nonpolar parts of molecules) is thought to play a key role in protein folding. Large nonpolar side chains would create a layer largely depleted of water when hydrophobic domains are brought together. However, this situation is based mainly on a consideration of van der Waals interactions between solutes and water. **Zhou *et al.*** (p. 1605) have performed molecular dynamics simulations of the BphC enzyme, a two-domain protein that collapses into a globular structure in which complementary hydrophobic faces align. Only a weak water depletion, with a water density about 10 to 15% lower than the bulk, was formed between the hydrophobic domains. The authors find that when electrostatic effects are artificially removed in their simulations, the dewetting transition reappears and the collapse transition occurs at a much faster rate.

Phytoplankton Feel the Heat

The marine pelagic ecosystem is the largest one on Earth, yet little is known how global warming might affect it. Phytoplankton make up the base of the marine food web and support the rest of the larger organisms in the oceans. **Richardson and Schoeman** (p. 1609; see the news story by **Stokstad**) studied the impact of climate change on the abundance of marine planktonic food web over large space and time scales in the Northeast Atlantic. Their analysis of more than 100,000 samples over 45 years shows that climate warming has increased in the abundance of phytoplankton in cooler regions and a decrease in warmer ones.

Ensuring Adequate Gas Supplies

In an uncertain world, survival may depend on leaving nothing to chance. In biochemical terms, the way to place a spontaneously occurring process under control is to make an enzyme that catalyzes the reaction. Biological membranes are inherently permeable to gases, such as oxygen, yet **Khademi *et al.*** (p. 1587; see the cover and the Perspective by **Knepper and Agre**) now describe a bacterial protein that functions as an ammonia channel. The crystal structure of AmtB reveals a vestibule where the water-soluble species NH_4^+ is deprotonated and a hydrophobic conduit enables NH_3 to cross the membrane. The human analog of AmtB is the well-known rhesus or Rh factor.

Take That Copper

Methanotrophic bacteria oxidize methane, and copper plays a central role in the metabolism of these organisms. However, their copper trafficking mechanism is not well defined. **Kim *et al.*** (p. 1612) have identified and determined the structure of methanobactin, a copper-sequestering small molecule from the methanotroph *Methylosinus trichosporium* OB3b. Structural similarities to iron

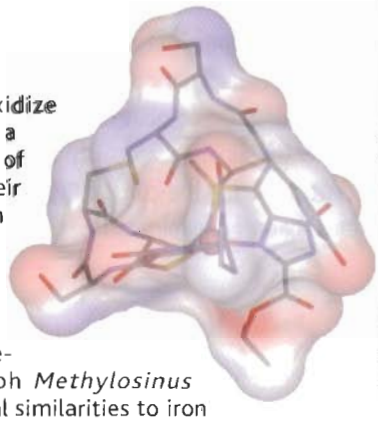

CONTINUED ON PAGE 1529